SCIENTIFIC REPORTS

OPEN

SUBJECT AREAS:
BATTERIES
SYNTHESIS

Received
30 December 2013

Accepted
27 January 2014

Published
6 March 2014

Correspondence and requests for materials should be addressed to X.L.H. (huxl@mail.hust.edu.cn) or Y.H.H. (huangyh@mail.hust.edu.cn)

Encapsulation of MnO Nanocrystals in Electrospun Carbon Nanofibers as High-Performance Anode Materials for Lithium-Ion Batteries

Bin Liu, Xianluo Hu, Henghui Xu, Wei Luo, Yongming Sun & Yunhui Huang

State Key Laboratory of Materials Processing and Die & Mould Technology, School of Materials Science and Engineering, Huazhong University of Science and Technology, Wuhan 430074, P. R. China.

A novel and controllable approach is developed for the synthesis of MnO nanocrystals embedded in carbon nanofibers (MnO/CNFs) through an electrospinning process. The as-formed MnO/CNFs have a porous structure with diameters of 100–200 nm and lengths up to several millimeters. When used as an anode material for lithium-ion batteries, the resulting MnO/CNFs exhibit superior electrochemical performances with high specific capacity, good cyclability, and excellent rate capability. The unique porous carbon nanofibers (PCNFs) can not only improve the contact area between the electrode and the electrolyte, but also alleviate the impact of the large volume effect of MnO during the electrochemical cycling. It is expected that the present synthetic strategy can be extended to synthesize other nanostructured oxides encapsulated in carbon nanofibers for extensive energy transfer and storage applications.

Owing to high energy density and long life, lithium-ion batteries (LIBs) have becoming the most promising energy-storage devices that are explored for upcoming electric vehicles (EVs) and hybrid electric vehicles (HEVs)[1–3]. Considering the increasing demands for large energy and power density currently, the electrode materials with high reversible capacity, good rate capability, and desirable cyclability are intensively investigated. Recently, transition metal oxides (TMOs) have become a potential research focus as promising anode materials (e.g., CoO[4–7], Co_3O_4[8–10], NiO[11–13], TiO_2[14–16], MoO_2[17–20], Mn_3O_4[21–23], and Mn_2O_3[24,25]) because of their higher capacities than graphite. Among TMOs, MnO has aroused much attention for high-performance LIBs, since it possesses high theoretical capacity (755 mAh g^{-1}), low voltage hysteresis comparatively (<0.8 V), low cost, and environmental benignity[26–36]. However, the application of MnO as practical electrode materials is hindered by many obstacles, including poor cycling stability, inferior rate capability, and huge volume expansion during the charge–discharge process[29]. Recently, the availability of carbonaceous materials has witnessed significant growth for improving the cycling performance. Meanwhile, nanostructured electrode materials fabricated by effective synthetic methodologies[33–37] have attracted so much attention in a variety of energy-storage devices because of the large specific surface area and short transport path for lithium ions and electrons. Therefore, decreasing the particle size, compositing with carbon and engineering appropriate morphologies of MnO are effective approaches to improve the electrochemical performances of MnO-based anodes for LIB applications.

Electrospinning has provided versatile and controllable fabrication strategies to construct well-defined one-dimensional (1D) carbon-coated composite fibers at a micro/nano-scale[38–42]. Moreover, some facile synthetic routes have been reported to achieve monodisperse Mn_3O_4 nanocrystals on a large scale[43–45]. Herein, we demonstrate the preparation of uniform MnO nanocrystals that are encapsulated in carbon nanofibers (CNFs) through electrospinning of Mn_3O_4 nanoparticles into CNFs and subsequent annealing in Ar/H_2 atmosphere. Benefiting from the synergetic effects of CNFs and MnO nanocrystals, the resulting composites of MnO/CNFs exhibit excellent electrochemical lithium-storage performance when used as the anode material in LIBs.

Results

The synthetic process for the MnO/CNFs composite is illustrated in Fig. 1. Firstly, monodisperse Mn_3O_4 nanoparticles with an average diameter of ~15 nm (Fig. 2) were prepared by a solvothermal method[45]. Then, the Mn_3O_4 nanoparticles dispersed in polyacrylonitrile/N, N-dimethylformamide (PAN/DMF) solutions were

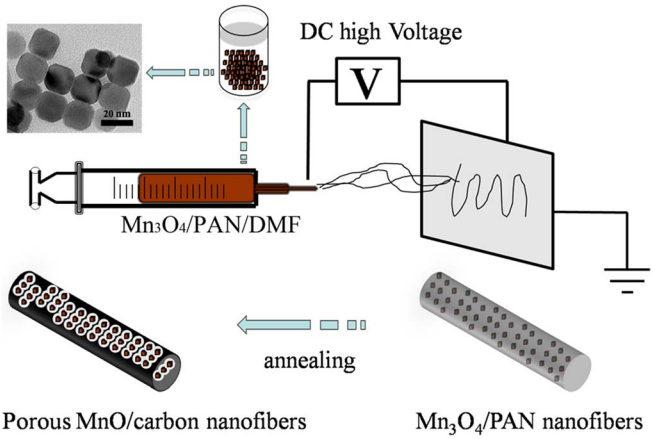

Figure 1 | Schematic illustration of the preparation process of monodisperse Mn_3O_4 nanoparticles encapsulated in porous carbon nanofibers. The precursor solution contains PAN (10 wt%) and Mn_3O_4 nanocrystals in DMF.

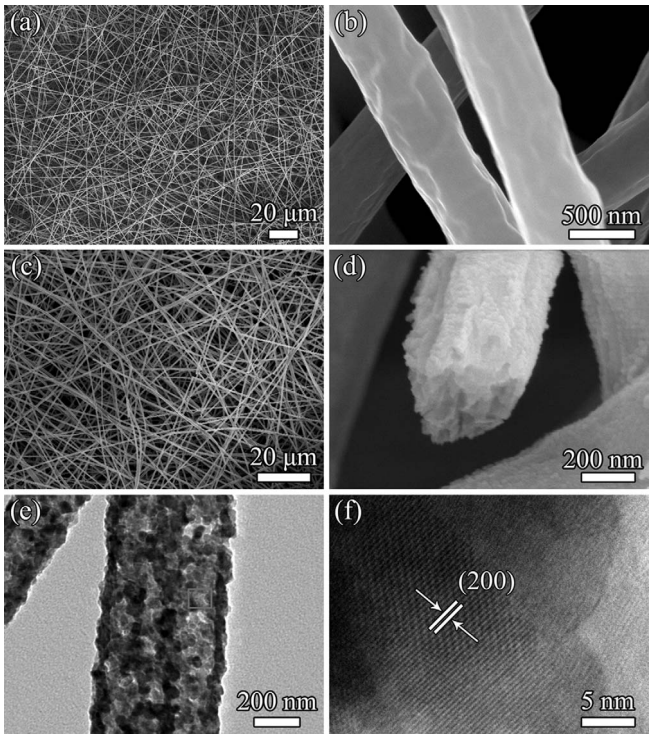

Figure 3 | Morphologies of the as-spun nanofibers and the porous after thermal treatment in Ar/H_2 at 500°C for 5 h. (a,b) FESEM images of the as-spun nanofibers; (c,d) the porous MnO/CNFs after thermal treatment in Ar/H_2 at 500°C for 5 h; (e) TEM image of the porous MnO/CNFs; (f) HRTEM image of the resulting porous MnO/CNFs corresponding to the area marked with a square in (e).

electrospun into nanofibers. The scanning electron microscope (SEM) image in Fig. 3a and 3b show that the as-spun Mn_3O_4/PAN composite nanofibers are smooth and continuous with diameters of 100–300 nm and lengths up to several millimeters. Previous research has already demonstrated that the nanofiber diameter is dominated by intricate interaction among the viscosity, surface tension, and conductivity of the electrospinning solution[39–42]. After thermal processing in Ar/H_2 at 500°C for 5 h, the fibrous shape and diameter maintained well, and no individual or accumulation of particles was observed (Fig. 3c and 3d). Fig. 3d and 3e shows the morphology of the product at a higher magnification, clearly indicating a large quantity of wormhole-like pores. The MnO nanoparticles are homogeneously encapsulated in the porous carbon nanofibers with the pore diameters less than 20 nm, which is in favor of contacting the electrolyte with active materials and the transfer of e^- and Li^+. Fig. 3f shows the high-resolution transmission electron microscopy (HRTEM) image for the MnO nanocrystals that are surrounded by a layer amorphous carbon. The lattice fringe with a spacing of 2.2 Å corresponds to the (200) plane of MnO. The porous characteristic of the MnO/CNFs product is further confirmed by nitrogen adsorption−desorption measurements. Fig. 4 displays the isothermal plot of the MnO/CNFs, which is a typical type IV isotherm of a mesoporous structure with a Brunauer−Emmett−Teller (BET) specific surface area as high as 79.8 $m^2 g^{-1}$. The pore size distribution (inset of Fig. 4) suggests that the MnO/CNFs product has numerous mesopores ranging from ~2 to 10 nm in diameter. It is expected that the electrode made of the resulting MnO/CNFs with high specific surface area and numerous mesopores will be available for access of the electrolyte to the internal active materials[6]. Meanwhile, the porous carbon network can not only buffer the volume change of MnO during cycling, but also maintain a continuous conductive network for the fast electron and Li-ion transportation, thus leading to enhanced electrochemical lithium-storage performances.

As shown in Fig. 5a, the X-ray diffraction (XRD) pattern of the MnO/CNFs product can be readily indexed to a pure phase of cubic MnO. The Raman shift of MnO (~362 and 645 cm^{-1}) and C (~1340 and 1585 cm^{-1}) can be clearly illustrated in the Raman spectrum (Fig. 5b)[41]. The representation of the D band with a high intensity suggests higher lithium-storage performance[43,44]. The composition and the surface electronic states of the MnO/CNFs product were explored by X-ray photoelectron spectroscopy (XPS) analysis. As shown in Fig. 5c and 5d, the elemental manganese and carbon are generated from MnO and the carbon nanofibers, respectively. The two signals at 641.2 eV for Mn $2p_{3/2}$ and 652.8 eV for Mn $2p_{1/2}$ are

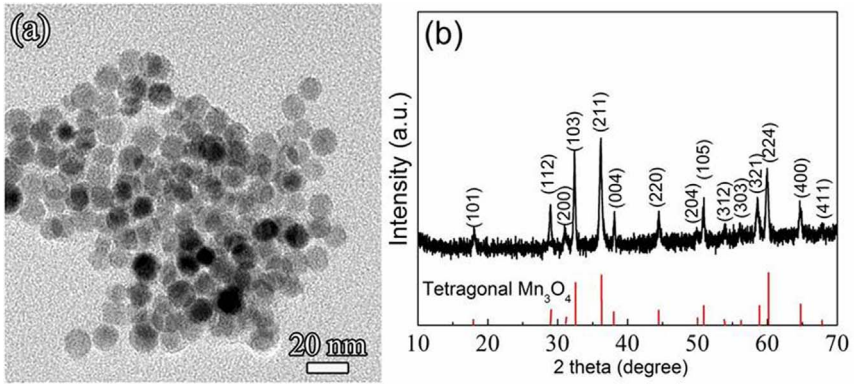

Figure 2 | Structural properties of Monodisperse Mn_3O_4 Nanocrystals. (a) TEM image; (b) XRD pattern.

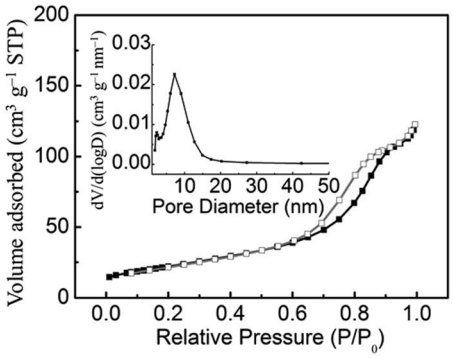

Figure 4 | Nitrogen adsorption and desorption isotherm of MnO/CNFs. Inset: the pore size distribution.

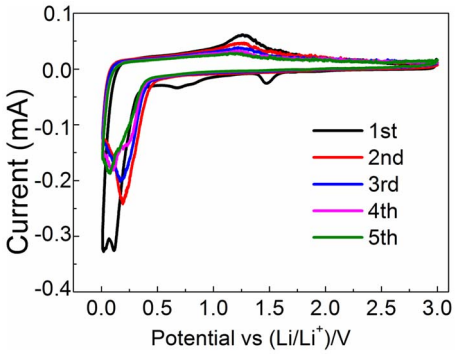

Figure 6 | Representative CV curves of the MnO/CNFs product at a scan rate of 0.1 mV s^{-1} in the voltage range of 3–0.01 V vs. Li/Li^+.

observed, which is characteristic of MnO[30]. The high-resolution C 1s spectrum can be deconvoluted into three peaks. The strong peak at 284.6 eV corresponds to the C−C bonds in the carbon nanofibers, while the weaker ones at 286.2 and 289.0 eV demonstrate the existence of some residual oxygen-bonded C atoms arising from the incomplete reduction/carbonization of organic substances at 500°C in the product[42]. The carbon content in the MnO/CNFs by thermogravimetric (TG) analysis is evaluated to be about 14.3 wt% (Fig. S1).

The lithium-storage properties of the as-prepared MnO/CNFs have been investigated by using the Li half-cells. Fig. 6 shows the cyclic voltammetry (CV) curves of the electrode made of the MnO/CNFs at a scan rate of 0.1 mV s^{-1} in the potential range of 3–0.01 V. In the first cycle, an obvious reduction peak at ~1.5 V can be assigned to the reduction of Mn^{3+} or Mn^{4+} to Mn^{2+}, which could be originated from a trace Mn_xO_y mixture from the partial oxidation of Mn^{2+} in the product[29]. Besides, another reduction peak at 0.70 V is observed, which is associated with the irreversible reactions between Li and MnO and the formation of a solid electrolyte interphase (SEI) layer. In the second cycle, however, the reduction peak at 0.70 V disappears, suggesting the formation of the SEI layer only in the first cycle. Moreover, the obvious cathodic peak close to 0.11 V corresponds to the complete reduction of Mn^{2+} to Mn^0, which shifts significantly to 0.2 V in the following cycles. In the anodic process, an evident oxidation peak at 1.25 V could be attributed to the oxidation of Mn^0 to Mn^{2+} [33]. From the second cycle on, the peaks in the scans are clearly overlapped, indicating the electrochemical reversibility and structural stability of the electrode.

In a control experiment (Fig. S2), we synthesized MnO nanoparticles by direct thermal treatment Mn_3O_4 nanocrystals under the same conditions for annealing of the MnO/CNFs. The XRD pattern (Fig. S2a) and the TEM (Fig S2b) image reveal that the particle sizes of these MnO particles range from 200 to 300 nm. The electrochemical performance of the MnO nanoparticles is much worse than that of the MnO/CNFs product. Although the electrode made of the bare MnO nanoparticles displays a high initial discharge capacity of 1016 mA h g^{-1} at a low current density of 100 mA g^{-1}, it decays rapidly to 309 mAh g^{-1} after only 20 cycles (see Fig. 7a).

Fig. 7b shows the representative discharge–charge curves of the MnO/CNFs electrode at a current density of 100 mA g^{-1} in potential range between 0.01 and 3 V. The initial discharge capacity of the electrode in the first discharge process is as high as 1380 mAh g^{-1}, which is much higher than the theoretical value (755 mAh g^{-1}) of MnO due to the conversion reaction. In the subsequent cycles, both of the discharge and charge curves gradually become shorter, due to

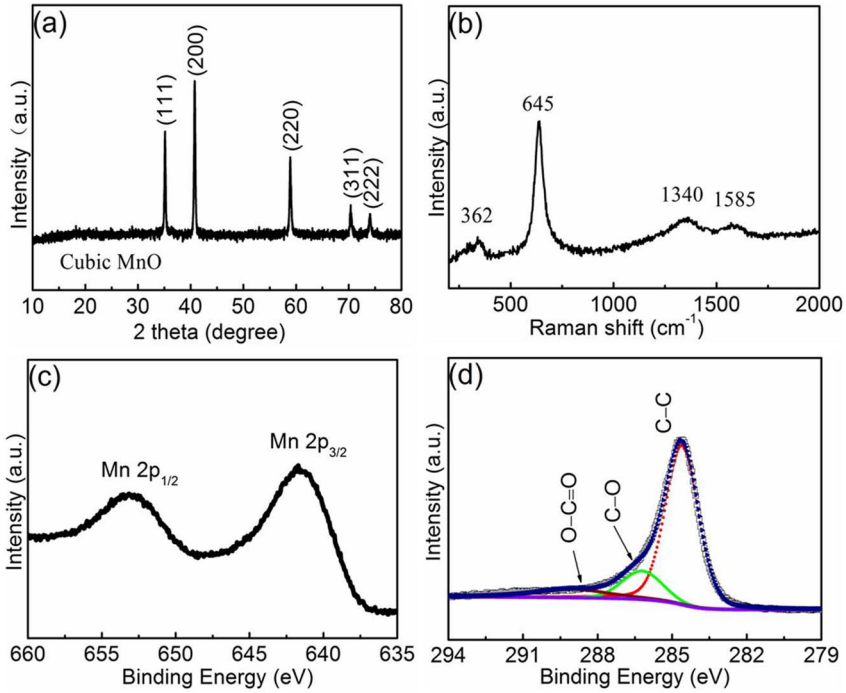

Figure 5 | Structural information of MnO/CNFs *via* XRD, Raman and XPS. (a) XRD pattern; (b) Raman spectrum; (c, d) XPS spectra.

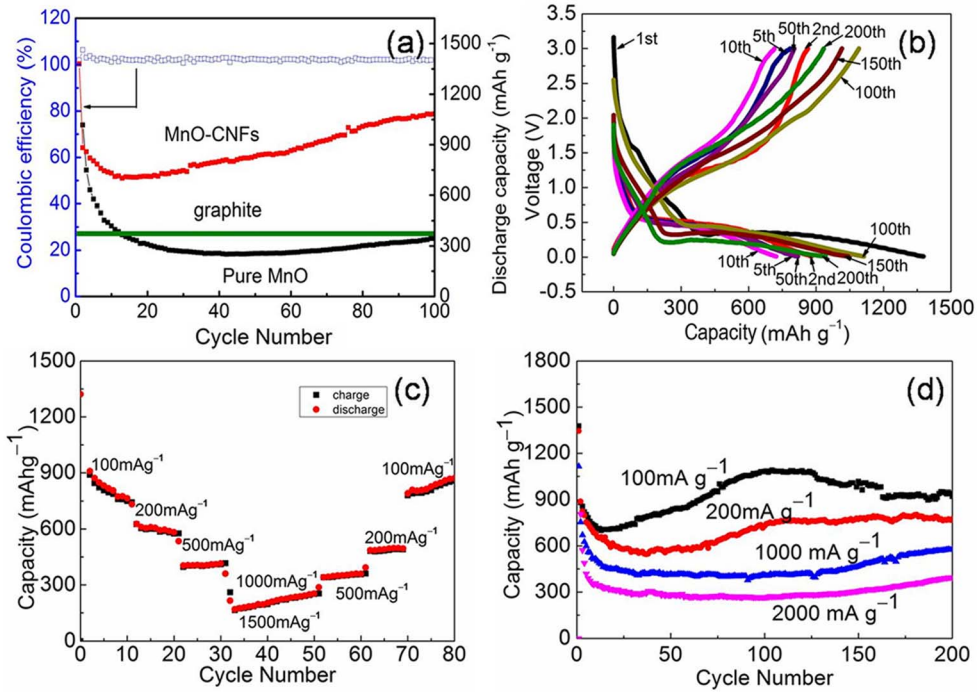

Figure 7 | Electrochemical performances of the products. (a) Capacity − cycle number curves of MnO/CNFs and bare MnO nanoparticles at a current density of 100 mA g^{-1}; (b) Galvanostatic discharge and charge curves at a current density of 100 mA g^{-1} cycled in the voltage range of 3–0.01 V vs. Li/Li^{+1}; (c) Rate performances of MnO/CNFs; (d) Cycling performance of the prepared MnO/CNFs electrode at various current densities of 100, 200, 1000, and 2000 mA g^{-1} (200 cycles).

the common capacity fading. However, the capacity starts to rebound after 10 cycles. This phenomenon that the capacity curve firstly drops and then increases has been observed in the previous work, which may be attributed to the new electrochemical reaction to form high-oxidation state products, nonuniform distribution of Mn cluster aggregation and reversibility improvement for the conversion reaction of manganese oxide through the thermal treatment process[29–32].

Fig. 7c and 7d shows the cycling behavior of the product at different current densities. Until 100 cycles at 100 mA^{-1}, the discharge capacity is as high as 1082 mAh g^{-1} with a Coulombic efficiency of 99%, indicating an excellent cyclic performance. Even at a high current density of 1000 mA g^{-1}, the specific capacity is up to 575 mAh g^{-1} after 200 cycles, still higher than the theoretical capacity of graphite (372 mAh g^{-1}). In addition, the MnO/CNFs electrode cycled at a high current density of 2000 mA g^{-1} presents similar electrochemical performances, which is better than that of previously reported MnO_2/CNTs[46]. As previously discussed in the literatures[29,47], the formation of defects in the electrodes during cycling can improve the conversion reaction kinetics, which can lead to the oxidation of Mn^{2+} to a higher oxidation state and the formation of a unique "U" shape.

Discussion

The excellent electrochemical performances of MnO/CNFs with unique nanoarchitectures comprising both MnO nanocrystals and numerous nanopores are reflected in the high specific capacity, good cyclability and superior rate capability. The as-fabricated products are not simply a result of the mixture of the two active substances of C and MnO. The effective design with the attractive merits achieved by assembling monodisperse MnO nanoparticles in carbon nanofibers reveals several unique characteristics. In our work, the increase of lager specific area and active sites may benefit from the porous one-dimension nanostructure, and therefore the ionic infiltration and specific capacity of the as-obtained MnO/CNFs are significantly improved. Also, the porous fibrous architecture made of C and MnO nanocrystals is in favour of relieving the strain induced by the volume change during the discharge–charge cycling and increasing the conductivity of the electrode in electrochemical processes, thus leading to the enhanced electrochemical performance[29–33]. Furthermore, the porosity of the MnO/CNFs available between the interconnected MnO nanoparticles and C contributes positively to Li-ion diffusion, and the high surface area also increases accessible sites on the surface of the electrochemically active material, leading to the excellent high-rate performance. The porous structure can also promote the diffusion of the liquid electrolyte into the bulk of the anode as well as providing fast transport channels for Li^+ ions[29,32]. The increased capacity of the MnO/CNFs (even larger than the theoretical capacity of MnO) may also be assigned to the interfacial Li storage as proposed by Maier and Tarascon[48,49]. and a part of high-oxidation state Mn-based products generated upon cycling, which is similar to the previous reports on other nanostructured Mn-based oxides[29,47]. Since our preparation technology is simple and rapid for uniform encapsulation of nanocrystals in nanofibers, it is an efficient way to design and fabricate high-performance electrode materials for next-generation rechargeable batteries.

In summary, we have successfully demonstrated a facile electrospinning method for the fabrication of nanocomposite MnO/CNFs, whereby monodisperse MnO nanocrystals of 15 nm are stabilized in porous CNFs. The unique 1D MnO/CNFs nanocomposite with porous structures exhibits high reversible capacity, excellent cyclability, and superior rate capability. Furthermore, the approach on the basis of CNFs as a structure support and a conductive medium for transition-metal oxide nanoparticles can be potentially extended to improve the electrochemical performance of other electrode materials in lithium-ion batteries.

Methods

Synthesis of MnO/CNFs. All reagents used were of analytical grade and used without any purification. Monodisperse Mn_3O_4 nanocrystals were prepared by a solvothermal method[45]. In a typical process, 5 mL of $Mn(NO_3)_2$ solution (50 wt%) was added to a Teflon-lined stainless autoclave containing 50 mL of oleylamine under

agitation. Then, the above solution was sealed and heated at 200°C for 24 h. After the reaction was cooled to room temperature, the Mn_3O_4 product was collected by centrifugation, washed with ethanol, and dried at 80°C in the oven. For the electrospinning process, a DMF solution containing PAN (10 wt%) and Mn_3O_4 nanoparticles (2 g) was stirred at 60°C for 24 h in order to obtain homogeneous viscous gray mixture. Then, the as-prepared precursor solution was loaded into a plastic syringe with a stainless steel nozzle. With a computer-controlled syringe pump (1 mL h^{-1}) and an applied voltage of 16 kV between the electrospinning jet and the collector (15 cm), the precursor solution was electrospun into nanofibers. The as-collected nanofibers were firstly stabilized in air at 280°C for 2 h and then annealed in a tube furnace at 500°C for 5 h in H_2 (5%)/Ar (2°C min^{-1}) to achieve the MnO/CNFs product.

Electrochemical measurements. The electrochemical performance of the as-prepared MnO/CNFs was examined using CR2032 coin type cells vs. Li with 1 M $LiPF_6$ in ethylene carbonate/dimethyl carbonate (1 : 1 by volume) and Celgard 2300 membrane as the separator. The working electrode consists of the 1D MnO/CNFs, acetylene black (Super P), and poly(vinyl difluoride) (PVDF) in a 70 : 20 : 10 weight ratio dispersed in N-methyl-2-pyrrolidone (NMP). The slurry was coated onto a copper foil and dried at 80°C in vacuum for 6 h before pressing. The as-prepared copper foil was cut into disk electrodes which are 8 mm in diameter and further dried at 80°C for 24 h in vacuum. The cells were assembled in an argon-filled glovebox with the water and oxygen concentration below 1.0 ppm. Cyclic voltammetry (CV) curves were measured on an electrochemical workstation (Shaghai Chen Hua Instruments, Model CHI660D) at a scanning rate of 0.1 mV s^{-1}. Galvanostatic charge–discharge measurements were performed on a Land Battery Measurement System (Land, China) under various current densities of 100, 200, 500, 1000, 1500 and 2000 mA g^{-1} in the cut off voltage range of 3.00–0.01 V vs. Li/Li at room temperature.

Other Characterizations. The crystal structure of the as-obtained materials was characterized by a PANalytical MultiPurpose Diffractometer, using Cu-Kα radiation irradiation (λ = 1.5406 Å) with 2θ ranging from 10° to 80°. The morphology of the samples was observed by field-emission scanning electron microscopy (FESEM) (FEI, Sirion 200). Transmission electron microscopy (TEM) (FEI, Model Tecna-20) and high-resolution transmission electron microscopy (HRTEM) (JEOL, Model JEM 2010F) were used to investigate the microstructural morphology. Thermogravimetric and differential thermal analyses (TG/DTA) were performed on a PerkinElmer Diamond TG/DTA apparatus in air at a heating rate of 10°C min^{-1}. X-ray photoelectron spectroscopy (XPS) measurements were carried out employing a VG MultiLab 2000 system with a monochromatic Al Kα X-ray source (ThermoVG Scientific). The nitrogen adsorption/desorption isotherms were measured at 77 K on a Micrometritics ASAP 2020 analyzer. Raman spectra were recorded on a Renishaw Invia spectrometer using an Ar laser at 514.5 nm.

1. Tarascon, J. M. & Armand, M. Issues and challenges facing rechargeable lithium batteries. *Nature* **414**, 359–367 (2001).
2. Dunn, B., Kamath, H. & Tarascon, J. M. Electrical energy storage for the grid: A battery of choices. *Science* **334**, 928–935 (2011).
3. Yuan, L. X. *et al.* Development and challenges of $LiFePO_4$ cathode material for lithium-ion batteries. *Energy Environ. Sci.* **4**, 269–284 (2011).
4. Poizot, P., Laruelle, S., Grugeon, S., Dupont, L. & Tarascon, J. M. Nano-sized transition-metal oxides as negative-electrode materials for lithium-ion batteries. *Nature* **407**, 496–499 (2000).
5. Sun, Y. M., Hu, X. L., Luo, W. & Huang, Y. H. Ultrathin CoO/graphene hybrid nanosheets: A highly stable anode material for lithium-ion batteries. *J. Phys. Chem. C* **116**, 20794–20799 (2012).
6. Sun, Y. M., Hu, X. L., Luo, W. & Huang, Y. H. Self-assembled mesoporous CoO nanodisks as a long-life anode material for lithium-ion batteries. *J. Mater. Chem.* **22**, 13826–13831 (2012).
7. Wu, F. D. & Wang, Y. Self-assembled echinus-like nanostructures of mesoporous CoO nanorod@ CNT for lithium-ion batteries. *J. Mater. Chem.* **21**, 6636–6641 (2011).
8. Li, Y., Tan, B. & Wu, Y. Mesoporous Co_3O_4 nanowire arrays for lithium ion batteries with high capacity and rate capability. *Nano Lett.* **8**, 265–270 (2008).
9. Wang, J. Y. *et al.* Accurate control of multishelled Co_3O_4 hollow microspheres as high-performance anode materials in lithium-ion batteries. *Angew. Chem. Int. Ed.* **52**, 6517–6420 (2013).
10. Liu, D. *et al.* Co_3O_4 nanocages with highly exposed {110} facets for high-performance lithium storage. *Sci. Rep.* **3**, 2543. DOI: 10.1038/srep02543 (2013).
11. Liu, X. *et al.* NiO nanocapsules with onion-like carbon shell as anode material for lithium ion batteries. *Carbon* **60**, 215–220 (2013).
12. Mai, Y. J., Shi, S. J., Zhang, D., Lu, Y. & Gu, C. D. NiO–graphene hybrid as an anode material for lithium ion batteries. *J. Power Sources* **204**, 155–161 (2012).
13. Hwang, S. G., Kim, G. O., Yun, S. R. & Ryu, K. S. NiO nanoparticles with plate structure grown on graphene as fast charge–discharge anode material for lithium ion batteries. *Electrochim. Acta* **78**, 406–411 (2012).
14. Luo, W., Hu, X. L., Sun, Y. M. & Huang, Y. H. Surface modification of electrospun TiO_2 nanofibers via layer-by-layer self-assembly for high-performance lithium-ion batteries. *J. Mater. Chem.* **22**, 4910–4915 (2012).
15. Ding, S. *et al.* Graphene-supported anatase TiO_2 nanosheets for fast lithium storage. *Chem. Commun.* **47**, 5780–5782 (2011).
16. Park, K. S. *et al.* Long-term, high-rate lithium storage capabilities of TiO_2 nanostructured electrodes using 3D self-supported indium tin oxide conducting nanowire arrays. *Energy Environ. Sci.* **4**, 1796–1801 (2011).
17. Shi, Y. F. *et al.* Ordered mesoporous metallic MoO_2 materials with highly reversible lithium storage capacity. *Nano Lett.* **9**, 4215–4220 (2009).
18. Sun, Y. M. *et al.* Morphosynthesis of a hierarchical MoO_2 nanoarchitecture as a binder-free anode for lithium-ion batteries. *Energy Environ. Sci.* **4**, 2870–2877 (2011).
19. Sun, Y. M., Hu, X. L., Luo, W. & Huang, Y. H. Self-assembled hierarchical MoO_2/graphene nanoarchitectures and their application as a high-performance anode material for lithium-ion batteries. *Acs Nano* **5**, 7100–7107 (2011).
20. Luo, W., Hu, X. L., Sun, Y. M. & Huang, Y. H. Electrospinning of carbon-coated MoO_2 nanofibers with enhanced lithium-storage properties. *Phys. Chem. Chem. Phys.* **13**, 16735–16740 (2011).
21. Sun, Y. M., Hu, X. L., Luo, W. & Huang, Y. H. Ultrafine MoO_2 nanoparticles embedded in a carbon matrix as a high-capacity and long-life anode for lithium-ion batteries. *J. Mater. Chem.* **22**, 425–431 (2012).
22. Li, L., Guo, Z., Du, A. & Liu, H. Rapid microwave-assisted synthesis of Mn_3O_4–graphene nanocomposite and its lithium storage properties. *J. Mater. Chem.* **22**, 3600–3605 (2012).
23. Gao, J., Lowe, M. A. & Abruña, H. D. Spongelike nanosized Mn_3O_4 as a high-capacity anode material for rechargeable lithium batteries. *Chem. Mater.* **23**, 3223–3227 (2011).
24. Deng, Y. F. *et al.* Porous Mn_2O_3 microsphere as a superior anode material for lithium ion batteries. *RSC Adv.* **2**, 4645–4647 (2012).
25. Qiu, Y. C. *et al.* Morphology-conserved transformation: synthesis of hierarchical mesoporous nanostructures of Mn_2O_3 and the nanostructural effects on Li-ion insertion/deinsertion properties. *J. Mater. Chem.* **21**, 6346–6353 (2011).
26. Liu, J. & Pan, Q. M. MnO/C nanocomposites as high capacity anode materials for Li-ion batteries. *Electrochem. Solid-State Lett.* **13**, A139–A142 (2010).
27. Qiu, D. F. *et al.* MnO nanoparticles anchored on graphene nanosheets via in situ carbothermal reduction as high-performance anode materials for lithium-ion batteries. *Mater. Lett.* **84**, 9–12 (2012).
28. Zhang, K. J. *et al.* Synthesis of nitrogen-doped MnO/graphene nanosheets hybrid material for lithium ion batteries. *ACS Appl. Mater. Interfaces* **4**, 658–664 (2012).
29. Luo, W., Hu, X. L., Sun, Y. M. & Huang, Y. H. Controlled synthesis of mesoporous MnO/C networks by microwave irradiation and their enhanced lithium-storage properties. *ACS Appl. Mater. Interfaces* **5**, 1997–2003 (2013).
30. Sun, Y. M., Hu, X. L., Luo, W. & Huang, Y. H. Porous carbon-modified MnO disks prepared by a microwave-polyol process and their superior lithium-ion storage properties. *J. Mater. Chem.* **22**, 19190–19195 (2012).
31. Mai, Y. J. *et al.* MnO/reduced graphene oxide sheet hybrid as an anode for Li-ion batteries with enhanced lithium storage performance. *J. Power Sources* **216**, 201–207 (2012).
32. Wang, T., Peng, Z., Wang, Y., Tang, J. & Zheng, G. MnO Nanoparticle@ mesoporous carbon composites grown on conducting substrates featuring high-performance lithium-ion battery, supercapacitor and sensor. *Sci. Rep.* **3**, 2693 (2013).
33. Sun, B., Chen, Z. X., Kim, H. S., Ahn, H. & Wang, G. X. MnO/C core–shell nanorods as high capacity anode materials for lithium-ion batteries. *J. Power Sources* **196**, 3346–3349 (2011).
34. Li, X. W. *et al.* Interconnected porous MnO nanoflakes for high-performance lithium ion battery anodes. *J. Mater. Chem.* **22**, 9189–9194 (2012).
35. Wu, M. S., Chiang, P. C. J., Lee, J. T. & Lin, J. C. Synthesis of manganese oxide electrodes with interconnected nanowire structure as an anode material for rechargeable lithium ion batteries. *J. Phys. Chem. B* **109**, 23279–23284 (2005).
36. Liu, S. Y. *et al.* Nanocrystal manganese oxide (Mn_3O_4, MnO) anchored on graphite nanosheet with improved electrochemical Li-storage properties. *Electrochim. Acta* **66**, 271–278 (2012).
37. Bruce, P. G., Scrosati, B. & Tarascon, J. M. Nanomaterials for rechargeable lithium batteries. *Angew. Chem. Int. Ed.* **47**, 2930–2946 (2008).
38. McCann, J. T., Li, D. & Xia, Y. Electrospinning of nanofibers with core-sheath, hollow, or porous structures. *J. Mater. Chem.* **15**, 735–738 (2005).
39. Thavasi, V., Singh, G. & Ramakrishna, S. Electrospun nanofibers in energy and environmental applications. *Energy Environ. Sci.* **1**, 205–221 (2008).
40. Li, D. & Xia, Y. N. Electrospinning of nanofibers: reinventing the wheel? *Adv. Mater.* **16**, 1151–1170 (2004).
41. Inagaki, M., Yang, Y. & Kang, F. Y. Carbon nanofibers prepared via electrospinning. *Adv. Mater.* **24**, 2547–2566 (2012).
42. Luo, W., Hu, X. L., Sun, Y. M. & Huang, Y. H. Electrospun porous $ZnCo_2O_4$ nanotubes as a high-performance anode material for lithium-ion batteries. *J. Mater. Chem.* **22**, 8916–8921 (2012).
43. Rogach, A. L. *et al.* Organization of matter on different size scales: Monodisperse nanocrystals and their superstructures. *Adv. Funct. Mater.* **12**, 653–664 (2002).
44. Jana, N. R., Chen, Y. & Peng, X. Size-and shape-controlled magnetic (Cr, Mn, Fe, Co, Ni) oxide nanocrystals via a simple and general approach. *Chem. Mater.* **16**, 3931–3935 (2004).
45. Li, P. *et al.* Mn_3O_4 Nanocrystals: facile synthesis, controlled assembly. and application. *Chem. Mater.* **22**, 4232–4236 (2010).
46. Xia, H., Lai, M. O. & Lu, L. Nanoflaky MnO_2/carbon nanotube nanocomposites as anode materials for lithium-ion batteries. *J. Mater. Chem* **20**, 6896–6902 (2010).

47. Sun, Y. M., Hu, X. L., Luo, W., Xia, F. F. & Huang, Y. H. Reconstruction of Conformal Nanoscale MnO on Graphene as a High-Capacity and Long-Life Anode Material for Lithium Ion Batteries. *Adv. Funct. Mater.* **23**, 2436–2444 (2013).
48. Balaya, P., Li, H., Kienle, L. & Maier, J. Fully reversible homogeneous and heterogeneous Li storage in RuO_2 with high capacity. *Adv. Funct. Mater.* **13**, 621–625 (2003).
49. Dedryvère, R. *et al.* Contribution of X-ray photoelectron spectroscopy to the study of the electrochemical reactivity of CoO toward lithium. *Chem. Mater.* **16**, 1056–1061 (2004).

Acknowledgments

This work was supported by Natural Science Foundation of China (Grant Nos. 21271078 and 51002057), PCSIRT (Program for Changjiang Scholars and Innovative Research Team in University, No. IRT1014), and NCET (Program for New Century Excellent Talents in University, No. NECT-12-0223).

Author contributions

X.L.H. designed the experiments. B.L. performed the experiments and data analysis. H.H.X., W.L. and Y.M.S. assisted with some of the experiments. X.L.H. and Y.H.H. guided the work and analysis. B.L. and X.L.H. wrote the paper.

Additional information

Supplementary information accompanies this paper at http://www.nature.com/scientificreports

Competing financial interests: The authors declare no competing financial interests.

How to cite this article: Liu, B. *et al.* Encapsulation of MnO Nanocrystals in Electrospun Carbon Nanofibers as High-Performance Anode Materials for Lithium-Ion Batteries. *Sci. Rep.* 4, 4229; DOI:10.1038/srep04229 (2014).